# Unconventional isotope effects, multi-component superconductivity and polaron formation in high temperature cuprate superconductors

Bussmann-Holder, A ; Keller, H

Abstract: Various unconventional isotope effect experiments on high-temperature cuprate superconductors are reported together with observations of multi-component order parameters. The experiments are interpreted in terms of multi-band superconductivity where polaron formation takes place which leads to a renormalization of the single particle energies. Experiments and theory comply consistently with each other.

DOI: https://doi.org/10.1088/1742-6596/108/1/012019

# Unconventional isotope effects, multi-component superconductivity and polaron formation in high temperature cuprate superconductors

Journal of Physics: Conference Series **108** (2008) 012019 doi:10.1088/1742-6596/108/1/012019

# Unconventional isotope effects, multi-component superconductivity and polaron formation in high temperature cuprate superconductors

**A Bussmann-Holder[1] and H Keller[2]**

[1]Max-Planck-Institut für Festkörperforschung, Heisenbergstr. 1, D-70569 Stuttgart, Germany
[2]Physik Institut der Universität Zürich, Winterthurerstr. 190, CH-8057 Zürich, Switzerland

**Abstract.** Various unconventional isotope effect experiments on high-temperature cuprate superconductors are reported together with observations of multi-component order parameters. The experiments are interpreted in terms of multi-band superconductivity where polaron formation takes place which leads to a renormalization of the single particle energies. Experiments and theory comply consistently with each other.

## 1. Introduction

The discovery of high temperature superconductivity in copper oxides [1] was motivated by the knowledge that copper is one of the strongest Jahn-Teller ions [2]. In addition, the intimate acquaintance of perovskite oxides led the search for high temperature superconductivity in the prototype system $La_{2-x}Sr_xCuO_4$ [1]. In Jahn-Teller systems the electronic degeneracy is lifted through a lattice distortion which – in turn – lowers the overall system energy [3]. Thus, a strong coupling between the lattice and the electronic degrees of freedom is a prerequisite for this physics. For cuprates, however, electron lattice interactions are frequently being ignored to be the origin of the electron (hole) pairing and high temperature superconductivity. Since isotope experiments in conventional superconductors have been the clue in identifying the pairing mechanism, a systematic study of isotope effects in cuprate high temperature superconductors (HTS's) can help in discerning the microscopic origin of the pairing mechanism together with determining the order parameter symmetry.

Oxygen isotope effect (OIE) experiments on HTS's have been carried through early on [4], and, especially the nearly absence of an isotope effect at optimum doping has been taken as evidence that the lattice is inoperative in the pairing. With decreasing doping, however, the OIE on the superconducting transition temperature $T_c$ increases and exceeds the BCS value considerably in the region where the crossover to antiferromagnetism takes place [4]. Besides of this rather unexpected behavior additional unconventional OIE's have been observed on the pseudogap temperature T* [5], the penetration depth [6 – 9], and the superconducting gap [10]. Since conventional electron-phonon coupling can neither explain the doping dependence of the isotope effect nor those on the penetration depth and T*, it is shown that polaron formation causes these effects where a Jahn-Teller mode is effective [11 – 13].

 

## 2. Oxygen isotope effect experiments on the superconducting transition temperature

OIE experiments on HTS's require special caution since small deviations in the doping level of exchanged samples mimic marginal isotope effects [14]. For this reason experiments for both isotopes have to be done under identical conditions, i.e., using the same starting material, the same growth conditions, the same thermal treatment. Also, it is necessary to control the OIE by means of back exchange in order to guarantee that spurious external influences are excluded. Only in this way real isotope effects are observable and reproducible [4].

The OIE on $T_c$ shows a generic tendency as a function of doping in all cuprate HTS's (Fig. 1), i.e. it increases continuously with decreasing doping to reach its maximum value on the border to the antiferromagnetic state where it is considerably larger than the BCS value [4].

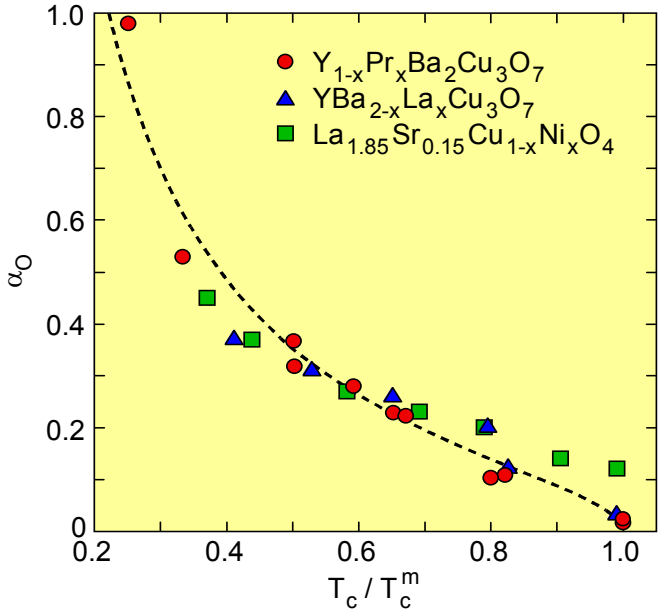


**Figure 1** OIE exponent $\alpha_O$ vs. $\overline{T}_c = T_C / T_c^m$ for various families of cuprate HTS ($T_c^m$ denotes the maximum $T_c$ for a particular family). Closed circles: $Y_{1-x}Pr_xBa_2Cu_3O_{7-\delta}$; open triangles: $YBa_{2-x}La_xCu_3O_7$; open squares: $La_{1.85}Sr_{0.15}Cu_{1-x}Ni_xO_4$. The dashed line corresponds to $\alpha_O = 0.25\sqrt{(1-\overline{T}_c)/\overline{T}_c}$ [15]. The references to the experimental data are given in [4].

This doping dependence of $\alpha_O = d\ln T_c / d\ln M_O$, where $M_O$ is the oxygen ion mass, has been explained theoretically within different models. Alexandrov [16] used a polaron model where the effective band mass causes the isotope effect. Rather analogous is the approach by Bill et al. [17] in contrast to the one by Kamimura and coworkers [18] where the isotope effect is a consequence of an anti Jahn-Teller effect. A completely different explanation was offered by Schneider and Keller where scaling relations were used to calculate the generic trend of the isotope effect [15]. Below a model is suggested which resembles the proposals of Refs. 16, 17, however with the distinction that not the effective mass is isotope dependent but the superfluid carrier density and, in addition, by extending the models of Refs. 16, 17 to a multi-component system [11 – 13].

Early on, the question was raised which oxygen ions cause the OIE on $T_c$. In order to address this issue, site selective OIE experiments have been carried through [19 – 21]. Here it is important to note that especially $YBa_2Cu_3O_{7-\delta}$ is an optimum candidate for these experiments since the oxygen isotope replacement at specific sites can be controlled thermally. To assure that specific sites have indeed been oxygen isotope exchanged, Raman scattering experiments have been performed where planar oxygen

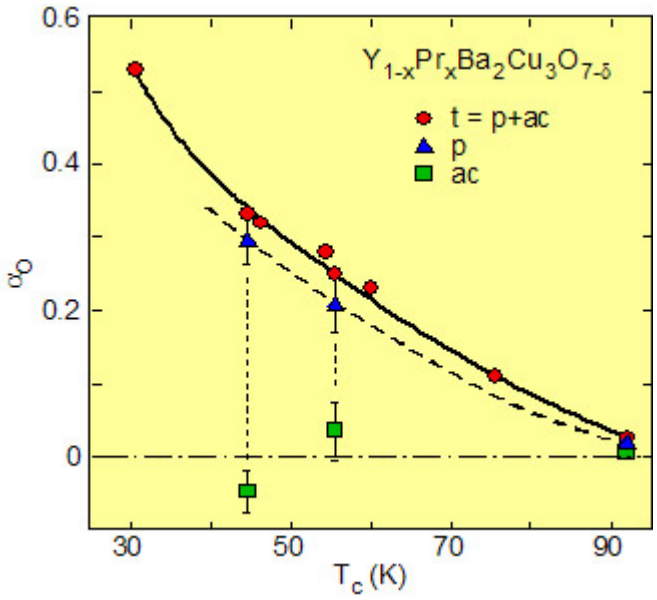


**Figure 2** Total (t) and partial (p, ac) oxygen-isotope exponent $\alpha_O$ as a function of $T_c$ for $Y_{1-x}Pr_xBa_2Cu_3O_{7-\delta}$ (t: all oxygen sites, p: planar oxygen sites; ac: apex and chain oxygen sites). Solid and dashed lines are guide to the eye. References to the data are given in [4].

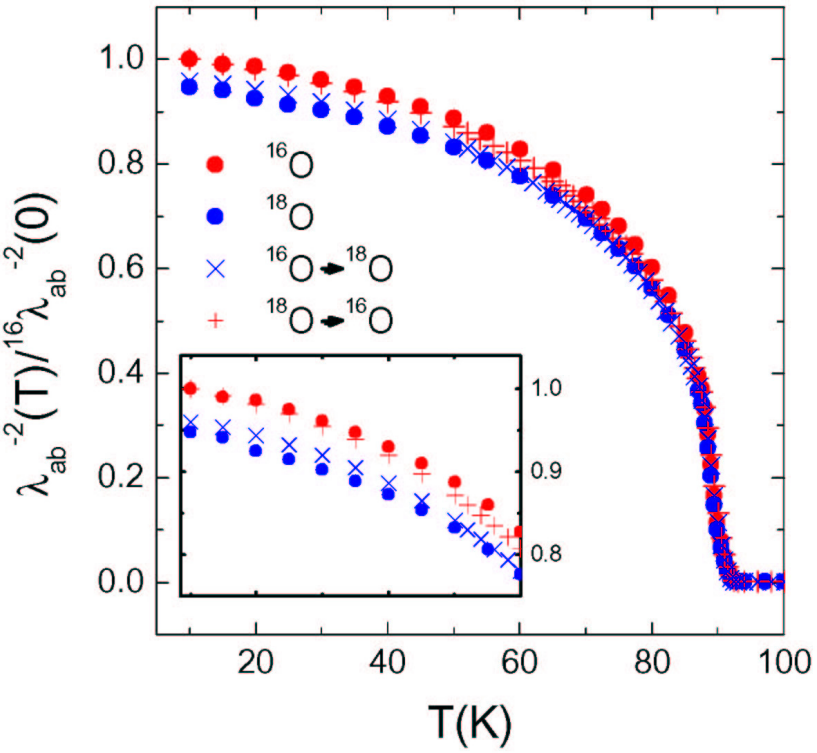


**Figure 3** Temperature dependence of $\lambda_{ab}^{-2}(T)$ normalized by $^{16}\lambda_{ab}^{-2}(0)$ for $^{16}O$ and $^{18}O$ substituted $YBa_2Cu_3O_{7-\delta}$ fine powder samples as obtained from low-field SQUID magnetization measurements. The inset shows the low-temperature region between 10K and 60K. The reproducibility of the oxygen exchange procedure was checked by the back exchange (crosses). After Ref. 9.

ions are easily distinguishable from chain and apical oxygen ions through their respective lattice mode frequencies. The results of this study are summarized in Fig. 2. As is obvious there, almost 100% of the OIE stems from the planar oxygen ions, while the chain and apical oxygen ions do not contribute to it. It can, however, from these experiments not be concluded that the latter oxygen ions are unimportant for high temperature superconductivity since their density of states is simply much smaller than the one stemming from the planar oxygen ions.

## 3. Oxygen isotope effect experiments on the magnetic penetration depth

Standard BCS theory relies on the Migdal theorem where the effective carrier mass m* is independent of the mass of the ions because of the giant mass difference between both. Since the magnetic penetration depth is proportional to m*, $1/\lambda^2(0) \propto \rho_s(0) \propto n_s/m^*$, no isotope effect on the magnetic penetration depth should exist. A break down of the Migdal theorem occurs, however, if the interaction between the lattice and the carriers is strong. In this case an isotope effect on the penetration depth should be observable. Various experimental techniques have been used to measure λ [4, 6 – 9]. While in SQUID magnetometry experiments fine powder samples were used [6, 7, 9], torque magnetometry requires single crystals [8], and for low-energy μSR experiments thin films are used [9]. As an example, Fig. 3 shows SQUID magnetization experiments which were performed on fine powders of $YBa_2Cu_3O_{7-\delta}$ [9]. As can be seen in Fig. 3, the in-plane magnetic penetration depth $\lambda_{ab}$

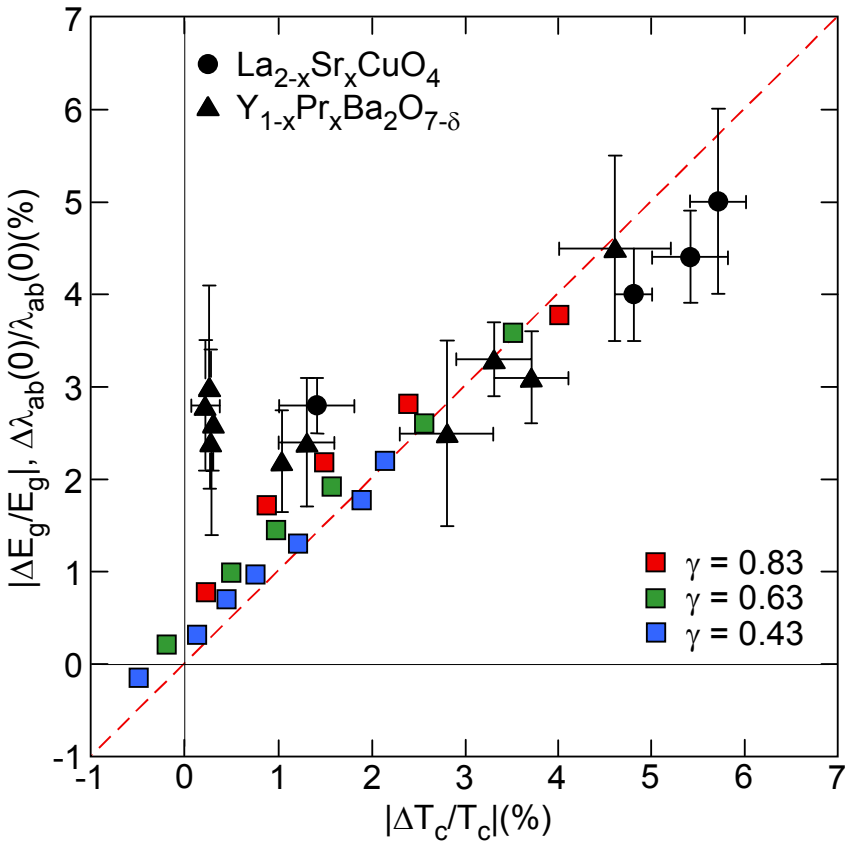


**Figure 4** Plot of the OIE shift $\Delta\lambda_{ab}(0)/\lambda_{ab}(0)$ vs. the OIE shift $-\Delta T_c/T_c$ for $La_{2-x}Sr_xCuO_4$, and $Pr_xY_{1-x}Ba_2Cu_3O_{7-\delta}$ using different experimental techniques and types of samples. The data are summarized in Table 1 of [4]. The dashed line corresponds to model calculations where the OIE on the average gap is also predicted. Note, that a negative OIE on the average gap is predicted at optimum doping and for overdoped systems. The differently shaded squares refer to different polaronic coupling constants γ as described in the text. After Ref. 11.

is clearly oxygen isotope dependent, where back exchange experiments have confirmed that the doping level of both isotope samples are the same. The penetration depth has been measured by the different techniques mentioned above and a summary of these results is given in Tables 1 and 2 of Ref. 4.

The above experiments have been performed systematically for different doping levels and compared to the isotope effect on $T_c$ (Fig. 4). An interesting correlation between both isotope effects results which is linear for nearly all doping levels, but deviates from this relation near optimum doping [4, 22]. An interpretation of the data in terms of polaronic effects is given in the same figure, where the experimentally observed deviations are, however, not reproduced [11].

## 4. Oxygen isotope effects on the superconducting energy gap

In conventional superconductors a universal relation between $T_c$ and the energy gap exists which naturally relates the isotope effect on $T_c$ to the one on the gap. In HTS's it is unclear that this relation holds since the isotope effect on $T_c$ is doping dependent, the dominant gap is of d-wave symmetry, and the order parameter is complex. The situation is thus rather non trivial and correspondingly experiments are highly desirable.

AC and DC magnetization experiments were carried through in a temperature range from 2K to 100 K on samples of $Y_{1-x}Pr_xBa_2Cu_3O_{7-\delta}$ with x=0.0, 0.2, 0.3, 0.45. From the in-plane magnetic penetration depth the average gap values for the above Pr composition were obtained [10]. In agreement with previous results for the superconducting gap a linear relation between these values and the corresponding values of $T_c$ is observed. $^{18}O$ isotope exchanged samples have been subject to the same thermal treatment, and for two compositions the back exchange experiments have been performed in order to guarantee that the doping level is unaffected by the oxygen isotope exchange. The results for the OIE on the gap are shown in Fig. 5 where the OIE on the gap is compared to the one on $T_c$ [10]. Interestingly, again a linear relation between both isotope effects exists which has been predicted by the polaronic model discussed below [11 – 13] and already shown in Fig. 4.

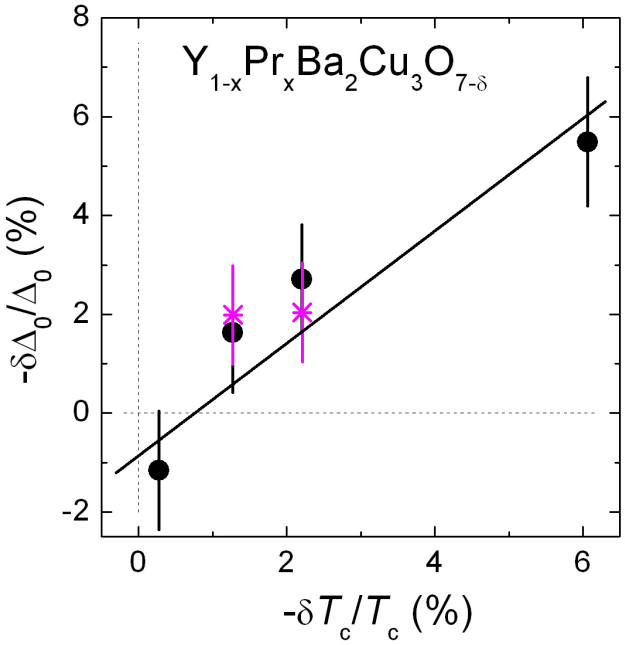


**Figure 5** Comparison of the oxygen isotope shift of the superconducting gap $\Delta_0$ to the one on the transition temperature $T_c$ for $Y_{1-x}Pr_xBa_2Cu_3O_{7-\delta}$ (x=0.0, 0.2, 0.3, 0.45). Circles refer to the experimental data, the solid line was obtained from model calculations [11 – 13] as discussed below. The stars represent back exchange data. After Ref. 10.

## 5. Oxygen isotope effects on the Néel temperature $T_N$ and the spin glass temperature $T_{SG}$

In order to examine lattice effects on the full phase diagram of HTS's OIE studies have been performed on the Néel state and the spin glass (SG) regime, i.e. on magnetic transition temperatures. Here zero field μSR experiments were carried through on the underdoped $La_{1.97}Sr_{0.03}CuO_4$ compound [23]. The oxygen isotope exchanged sample undergoes the transition to the SG phase at higher temperature than the $^{16}O$ sample, i.e., the OIE is sign reversed as compared to the one on $T_c$ and $\lambda_{ab}$ (Fig. 6).

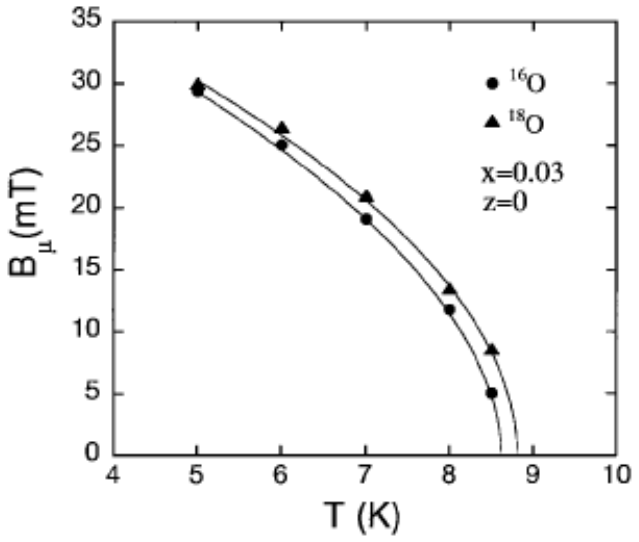


**Figure 6** Temperature dependence of the internal magnetic field at the muon site $B_\mu$ for the $^{16}O$ and $^{18}O$ samples of $La_{1.97}Sr_{0.03}CuO_4$. Solid lines represent fitted curves to the power law $B_\mu(T)=B_\mu(0)(1-T/T_{SG})^n$. After Ref. 23.

An interpretation of these results lies again in polaron formation since mobile carriers are much more effective in destroying the antiferromagnetic order than the static ones. In analogy to the spin glass transition also the Néel transition temperature is enhanced for the heavier isotope as compared to the $^{16}O$ samples [24]. Since this transition is tied to the insulating state, a reduction of the kinetic energy can explain this sign reversal of the isotope effect. Such a kinetic energy effect can again be caused by polaronic band renormalizations.

## 6. Mixed order parameters in HTS's

Early on it has been argued by Müller [25] and Müller and Keller [26] that the order parameter in HTS's is more complex than single simple d-wave type. Based on various experiments which are not consistent with a d-wave order parameter, they suggested that a substantial s-wave component must be present which is most pronounced along the crystallographic c-direction.

In order to test these early proposals, low field μSR experiments have been performed on single crystals of $La_{1.83}Sr_{0.17}CuO_4$ [27], $YBa_2Cu_3O_{7-\delta}$ [28], and $YBa_2Cu_4O_8$ [29]. As already mentioned above, the measurement of the penetration depth enables to determine the superconducting order parameter symmetry. For $MgB_2$, for instance, an inflection point in the temperature dependence of the penetration depth has provided clear evidence for the existence of two gaps [30]. Of particular importance for cuprates is the use of single crystals since then the gap symmetry can be tested along all three crystallographic directions. For $La_{1.83}Sr_{0.17}CuO_4$, only the in-plane penetration depth $\lambda_{ab}$ was measured [27]. The results are shown in Fig. 7 for different field strengths.

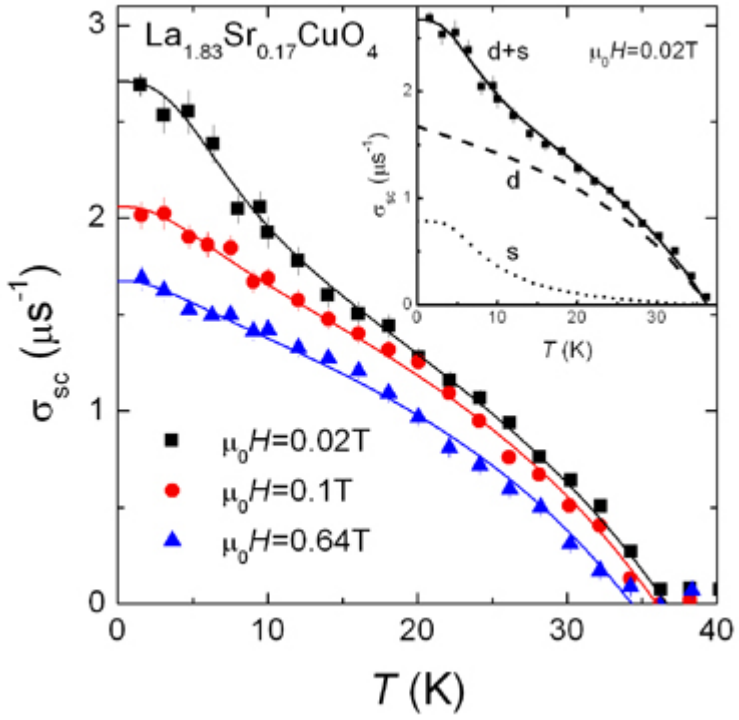


**Figure 7** Temperature dependence of the μSR relaxation rate $\sigma_{sc} \propto \lambda_{ab}^{-2}$ of single crystals of $La_{1.83}Sr_{0.17}CuO_4$ measured at field strengths of 0.02, 0.1 and 0.64 Tesla. Lines in the main figure and the inset represent calculations using a two gap model. The dashed and dotted lines in the inset show the individual contributions from the d- and s-wave gap. After Ref. 27.

For all field strengths, an inflection point appears at low temperatures which can only be explained by assuming that a small gap coexists with a larger one. Even though the gap symmetries remain arbitrary from a first analysis of the experiments, the field dependence of the individual components clarifies that the smaller gap has s-wave symmetry while the larger one is of d-wave symmetry. In order to find out whether this property is generic to cuprates or remains an exception to $La_{1.83}Sr_{0.17}CuO_4$, the two above mentioned compounds with completely different structures have been measured by the same method. In both compounds it was, in addition, possible to separate the penetration depth into three components referring to the crystalline a, b, and c directions [28, 29]. The results for $YBa_2Cu_3O_{7-\delta}$ and $YBa_2Cu_4O_8$ are shown in Figs. 8a and 8b.

In both systems, the μSR relaxation rates $\sigma_a \propto \lambda_a^{-2}$, and $\sigma_b \propto \lambda_b^{-2}$, exhibit again an inflection point at low temperatures, the signature of two gap superconductivity. The analysis of the data revealed that a small s-wave gap coexists with a large d-wave gap in the planes. Along the c-direction the situation is completely different since here the inflection point is missing and saturation occurs rapidly with decreasing temperature. Such a behavior is typical for a single s-wave order parameter. From these experiments it must be concluded that s+d wave symmetry of the order parameter in the $CuO_2$ planes is generic to HTS and that s-wave symmetry is realized along the c-direction even though a complete decoupling from the d-wave order parameter is not possible. This must, however, be too small to be detected experimentally.

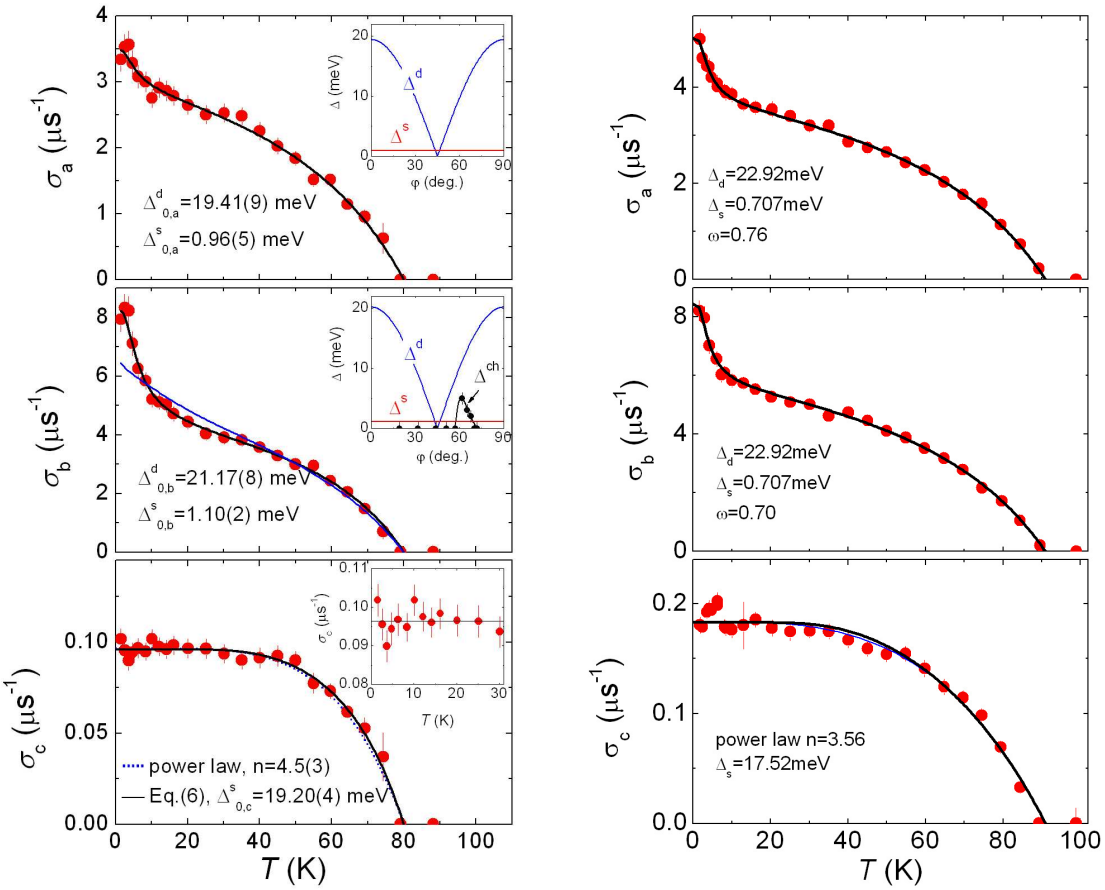


**Figures 8** a) (left panel) Temperature dependence of the μSR relaxation rate $\sigma_a \propto \lambda_a^{-2}, \sigma_b \propto \lambda_b^{-2}$, and $\sigma_c \propto \lambda_c^{-2}$ of single crystals of $YBa_2Cu_4O_8$ measured along the three principal crystallographic directions a, b, c. The insets to the figures show the individual contributions from the s- and d-wave gap. In the b-directions also the contribution from a possible chain related gap is plotted. The full lines are obtained as outlined in Ref. 29, the dashed lines result from a power law dependence [29]. b) (right panel) Temperature dependence of the μSR relaxation rate $\sigma_a \propto \lambda_a^{-2}, \sigma_b \propto \lambda_b^{-2}$, and $\sigma_c \propto \lambda_c^{-2}$ of single crystals of $YBa_2Cu_3O_{7-\delta}$ measured along the three principal crystallographic directions a, b, c. The lines are results from model calculations as discussed in [28].

## 7. Polaronic effects in HTS's

The above presented experimental results are all difficult to reconcile within a single component approach based on purely electronic mechanisms. Besides of these isotope experiments and the evidence for multiple order parameters, strain induced enhancements of $T_c$ [31] have been reported together with the occurrence of substantial phonon mode anomalies in the superconducting regime [32]. Experiments which test local properties have found that the bond length and angles vary periodically whereby dynamic superstructures are formed [33]. Another isotope effect within the phase diagram was observed on the onset temperature T* for stripe formation [5]. This OIE is sign reversed as compared to the one on $T_c$ and huge. All these data can only be explained if lattice effects are incorporated in the theoretical modeling. These lattice effects must, however, be different from conventional electron-phonon interactions as considered within BCS theory, since they must occur locally with doping dependent strength. In addition, the two components which are involved, have to

be specified, where theoretically the most likely candidates are the $CuO_2$ planes and the c-axis related almost insulating structural elements which resemble closely dielectrics.

While the undoped parent compounds are insulating antiferromagnets, doping rapidly destroys this order. Due to the oxygen ion configurational instability holes enter the oxygen ion p-states to form new in-gap electronic states. Obviously, doping causes a mismatch in all involved energy scales since lattice and charge mismatch together with the loss of the long range antiferromagnetic order are a consequence. In order to compensate for this energetically unfavorable situation local lattice distortions take place in the vicinity of the doped holes, i.e., polaron formation accompanies the additional charge (Fig. 9) [13].

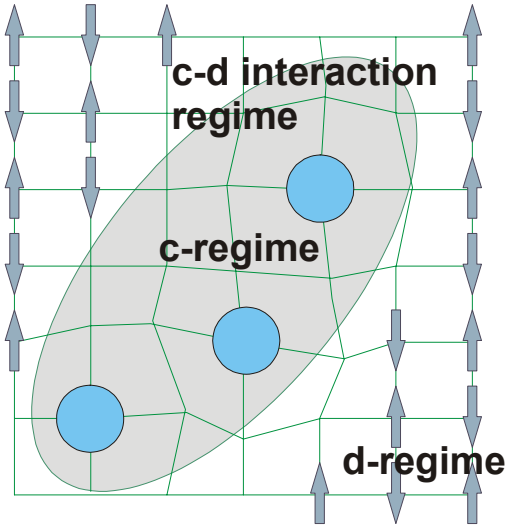


**Figure 9** Schematic representation of *c* and *d* dominated regimes. After Ref. 13.

One can thus differentiate two spatially varying regimes, the c-regime, which is charge rich and characterized by large local lattice distortions, and the d-regime, where antiferromagnetic fluctuations persist [13]. At high temperatures these locally distorted areas will form a polaron liqiud [34], where a random distribution of the c-regions occurs. Since huge strain fields are a consequence of dynamical local distortions, an energy lowering can be achieved by forming patterns or arrays like, e.g., stripes (Fig. 10).

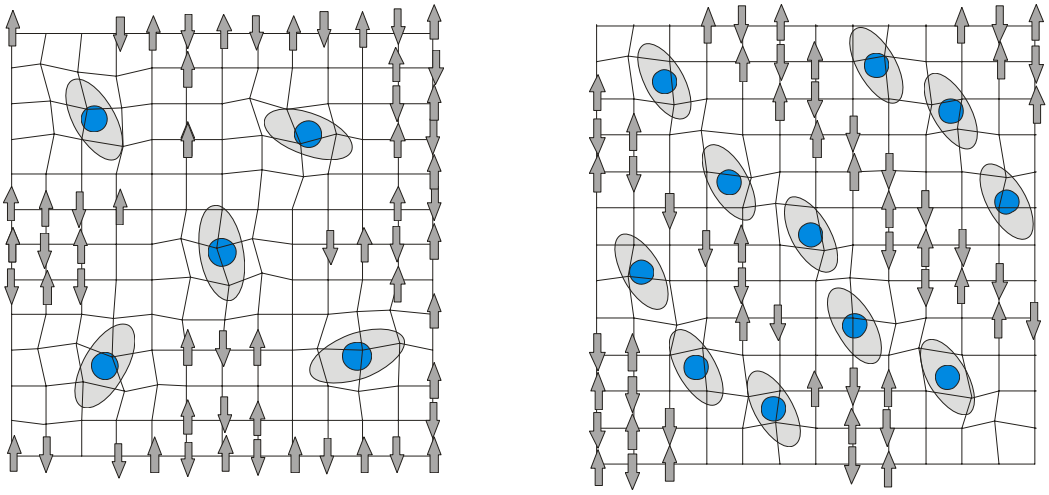

**Figures 10** Left panel: disordered polaron gas; right panel: ordered polaron liquid. After Ref. 13.

The two components, charge rich and spin rich ones, are not isolated from each other but interact through charge transfer and lattice distortions by means of which they get coupled (Fig. 11) [35].

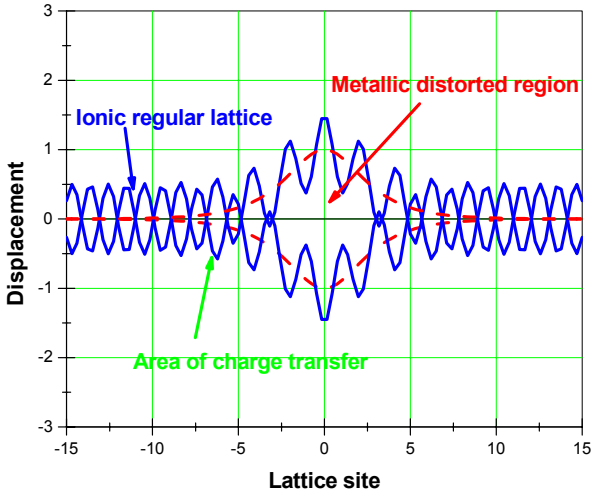


**Figure 11** Calculated displacement pattern based on an electron-phonon interaction model where the notations of the different regimes are the same as in Fig. 9. After Ref.13.

Electronically, two p-d hybridized bands are formed where one is related to the doped p-holes and the other to the lower Hubbard band. The charge transfer between both bands shifts the lower band in the vicinity of the Fermi surface while the dispersion of the other band is renormalized to lower kinetic energy. Formally, the two considered components can be described by the separate Hamiltonians [10]:

$$H_C = \sum_{j,\sigma} E_{C,j} c^+_{C,j} c_{C,j} + \sum_{i,j} [\tfrac{1}{2} M_i \dot{x}_i^2 + \frac{1}{2} c x_i^2 - g x_i (n_{j\uparrow} + n_{j\downarrow})] \quad (1)$$

$$H_{AB} = \sum_{j,\sigma} E_{AB,j} c^+_{AB,j\sigma} c_{AB,j\sigma} + U \sum_j n_{j\uparrow} n_{j\downarrow} + \sum_{i,j,\sigma} T_{ij} c^+_{AB,j\sigma} c_{AB,j\sigma} \quad (2)$$

where $H_C$ refers to the c-axis related elements and $H_{AB}$ to the $CuO_2$ planes. In both equations $c^+$, $c$ are electron creation and annihilation operators with band energies $E$ and density $n$, $M_i$ is the ionic mass of ion $i$, where typically the oxygen ion is referred to if not otherwise stated. $x$ is the site $i$ dependent local oxygen ion displacement and $g$ the local electron lattice coupling in the c-axis channel. $U$ is the onsite Coulomb repulsion and $T$ the transfer integral in the planes. As long as the system is undoped both equations are uncoupled. With doping, however, coupling is switched on due to local displacements. These facilitate that electronic states in the planes start to mix with those along the c-axis which is described by [35]:

$$H_{ABC} = \sum_{j,\sigma} \hat{T}_{ABC,j} c^+_{AB,j} c_{C,j} + h.c. \quad (3)$$

where $T$ depends explicitly on the lattice. As already outlined above the electron lattice coupling is treated on a polaronic level which admits to decouple lattice and electronic degrees of freedom through a Lang-Firsov transformation [36]. This technique introduces renormalizations of all quantities in the above equations (1 – 3) [35], where the most important ones are a reduction of $U$ which can even become attractive, a density-density interaction between c-axis and ab-plane related states and an exponential band narrowing through the hopping integrals.

The Hamiltonians given in equations (1 – 3) can be mapped on an effective two band model with interband interactions, which can be cast into a two-band BCS type Hamiltonian. Consequently, two superconducting gaps appear which are coupled and have to be solved self-consistently as a function of temperature. While the plane related gap has d-wave character, the c-axis related gap is a consequence of strong electron lattice interactions only and thus of s-wave symmetry. The gap coupling has the important effect that both symmetries are always mixed, i.e., the plane related d-wave gap adopts s-wave character whereas the c-axis gap acquires a d-wave admixture.

## 8. Results

The first and well known result of two-gap superconductivity is that $T_c$ experiences enormous enhancements [37] caused by the interband coupling only (Fig. 12a).

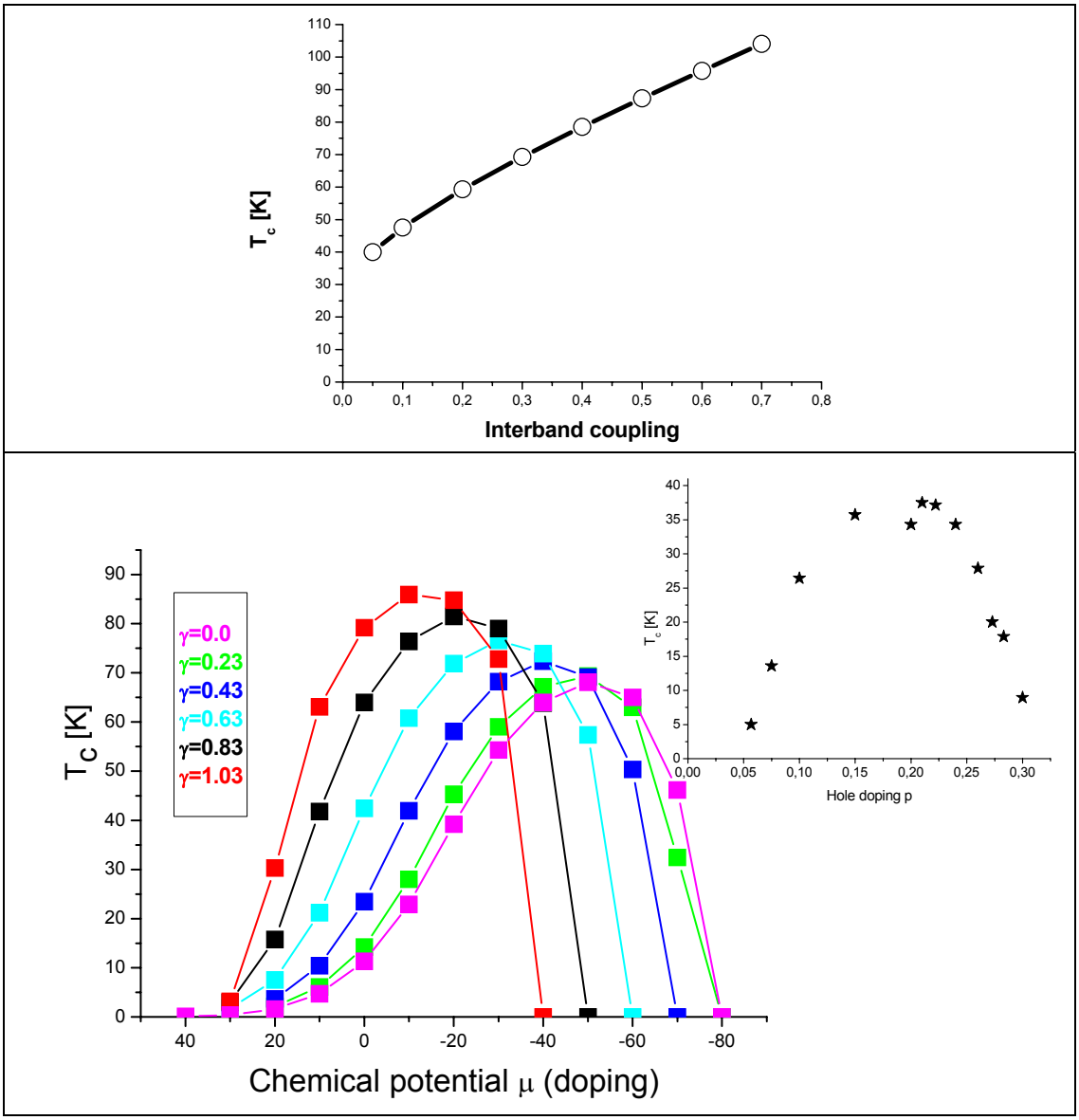


**Figures 12** a) (upper panel) dependence of $T_c$ on the interband coupling; b) (lower panel) $T_c$ as a function of doping for various polaronic coupling constants γ as indicated in the figure. The inset to the figure shows the experimental doping dependence of $T_c$ $La_{2-x}Sr_xCuO_4$. For details see Ref. 13.

Thus, a doubling of $T_c$ is easily achieved within the weak coupling limit. An additional enhancement effect stems from the polaronic coupling which yields a 30% increase in $T_c$ if the coupling is sufficiently strong (Fig. 12b) [13]. Note, that the doping dependence of $T_c$ is well reproduced by the model calculations. As detailed above two order parameters with different pairing symmetries result from this approach [37]. The model calculations are compared to data obtained from Andreev reflection [38] in Figs. 13 a and b, where in 13b the comparison is done with respect to the

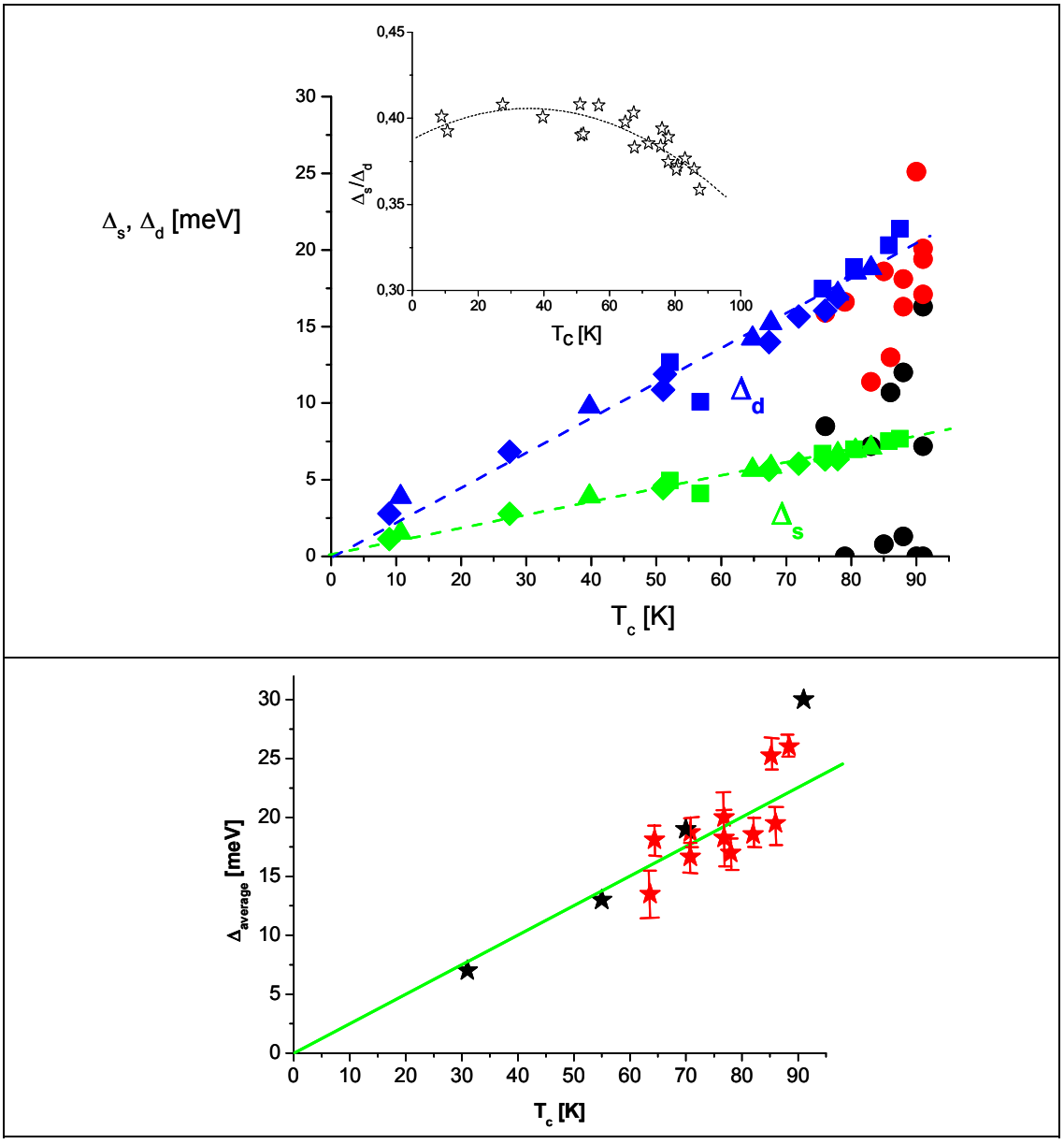


**Figures 13** a) (upper panel) Calculated dependence of the s- (light shaded symbols) and d-wave gaps (heavy shaded symbols) on $T_c$. The grey and black circles are experimental data from Ref. 38 for $YBa_2Cu_3O_{7-\delta}$. The various symbols used for the calculated results refer to different values of the polaronic coupling $\gamma$. The inset to this figure shows the ratio of the s-wave gap with respect to the d-wave gap as a function of $T_c$. b) (lower panel) The average gap $\Delta_{average}$ as a function of $T_c$. The line corresponds to model calculations, the black stars are from Ref. 10 for $Pr_{1-x}Y_xBa_2Cu_3O_{7-\delta}$, the grey ones from Ref. 38 for $YBa_2Cu_3O_{7-\delta}$.

normalized gap $\Delta = \sqrt{\Delta_d^2 + \Delta_s^2}$ and the new data [10] reported in the experimental part of this contribution.

The calculations predict a linear relation between $T_c$ and the averaged gap [13], which seems to be fulfilled experimentally. Simultaneously, the polaronic renormalization of the single particle energies leads to an isotope effect on $T_c$, the gap, and the penetration depth, which has already been shown in the first part. Important, however, is the fact that not all hopping integrals contribute equally to the isotope effects. The direct nearest neighbor hopping carries the wrong isotope effect while the second nearest neighbor hopping shows the same tendency with doping as observed experimentally [11 – 13]. An additional support to this trend stems from the inter-planar hopping term which then almost reproduces the experimentally observed doping dependence correctly (Fig. 14).

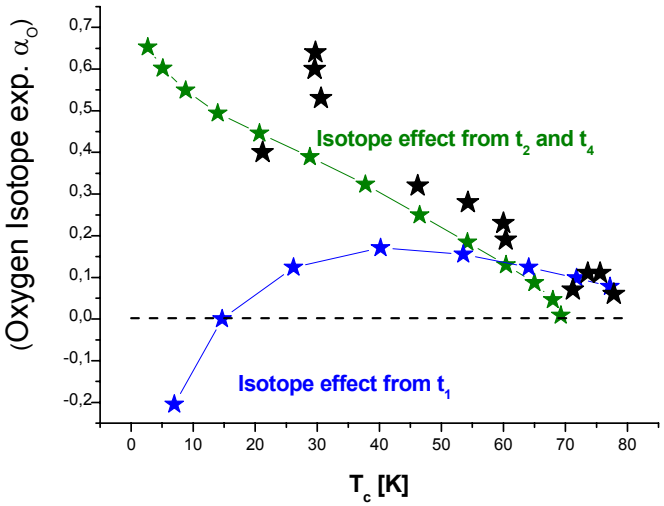


**Figure 14** The oxygen isotope exponent $\alpha_O$ as a function of $T_c$. The small dark stars refer to the calculated isotope exponent when only the nearest neighbor hopping integral $t_1$ is renormalized, the small grey stars are calculated points where both, second nearest neighbor and interplanar hopping integrals, $t_2$, $t_4$, are renormalized. Big black stars are experimental data points for $Y_{1-x}Pr_xBa_2Cu_3O_{7-\delta}$ [4]. After Refs. 10, 13.

Note, that values of the oxygen isotope exponent $\alpha_O$ of the order of 1 and larger are not reproduced by this approach. While important consequences also arise from the relation of the nearest to the second nearest neighbor hopping term which can be related to strain effects on $T_c$ [10, 13], we concentrate here on one further aspect of the model only. This relates to the experimental observation of the coexistence of the two order parameters which has been addressed above. From the calculated gaps the penetration depth can be derived which in turn can be compared to the experimentally observed one [39]. This is shown in Figs. 15 as a function of the magnetic field strengths.

The agreement between experiment and theory is certainly in support of the model. From the field dependence of the two components (Fig. 16) it can clearly be concluded that one is of s-wave symmetry while the other has d-wave symmetry, a fact that was not easily deductible from the experimental data alone.

## 9. Summary and conclusions

In this paper we have shown that HTS's show a variety of unusual isotope effects which can neither be explained within standard BCS theory nor understood within purely electronic models. In addition, two component superconductivity with mixed order parameter symmetries is realized where especially

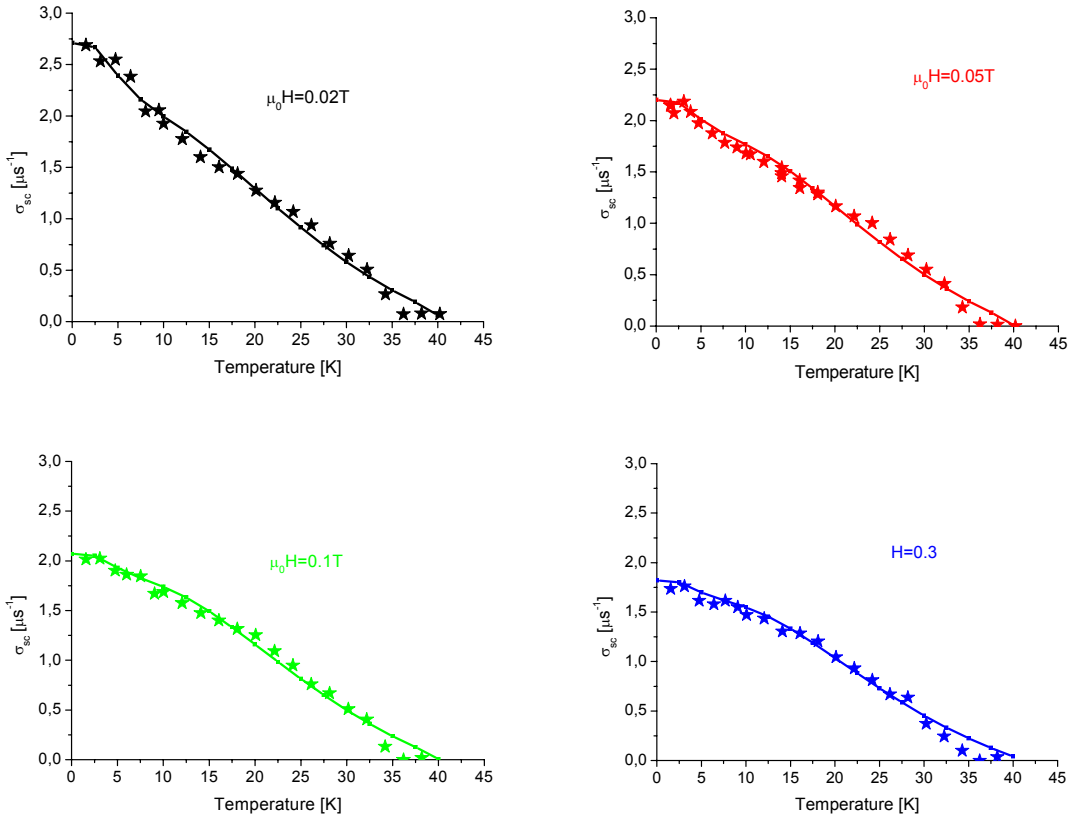


**Figure 15** Comparison of calculated μSR relaxation rate $\sigma_{sc} \propto \lambda_{ab}^{-2}$ (full lines) to experimental data (stars) of $La_{1.83}Sr_{0.17}CuO_4$ for different field strengths [27]: black: 0.02T, red: 0.05T; green: 0.1T; blue: 0.3T. After Ref. 39.

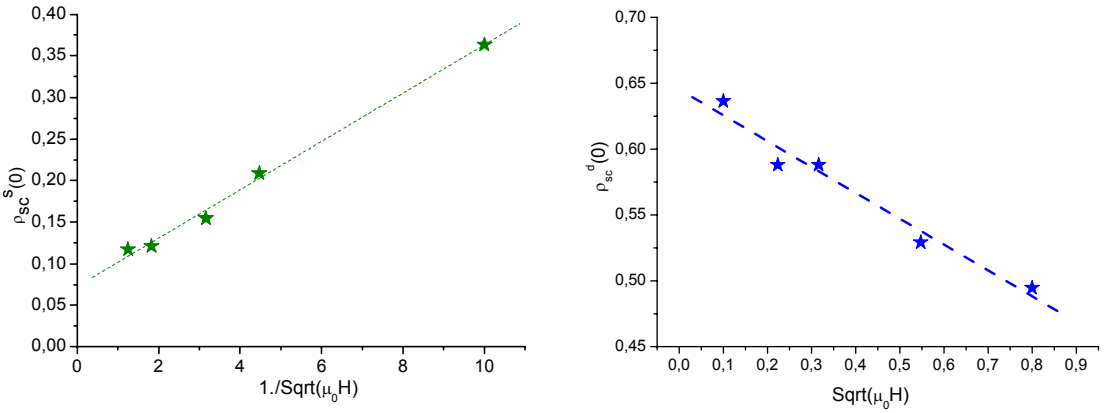


**Figure 16** The calculated field dependence of the individual contributions of the normalized superfluid density $\rho_{sc}$. In the left panel the d-wave contribution is shown, while the right panel shows the s-wave part. The stars represent experimental data of single crystals of $La_{1.83}Sr_{0.17}CuO_4$ from Ref. 27. After Ref. 39.

remarkable is the predominantly s-wave order parameter along the c-axis. This observation points to important consequences for HTS's since not only the $CuO_2$ planes play an important role, but the c-axis order parameter confirms the 3D nature of HTS's. The interpretation of the results in terms of a multi-component model with strong polaronic coupling provides a natural and consistent explanation of the experimental data. The final point to be addressed is the question which lattice distortions cause these effects. This question can be answered from the doping dependence of the isotope effect where we have shown that the second nearest neighbor hopping integral together with the inter-planar one yield the correct isotope effect. From this result it must be concluded that the OIE can not be caused by a breathing or a half breathing mode, but only by a $Q_2$ Jahn-Teller type mode [11 – 13] (Fig. 17) which is also consistent with the interpretation of EPR data in terms of a three spin polaron [40].

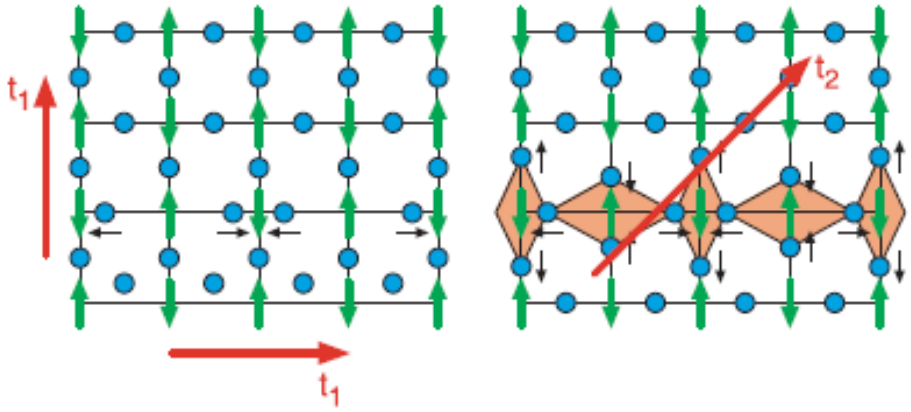


**Figure 17** The relevant ionic displacements which are either dominated by the nearest ($t_1$) or second nearest ($t_2$) hopping integrals. The circles represent the oxygen ions, the grey arrows are copper spins with antiferromagnetic order. The black arrows (left panel) indicate the displacement of the half-breathing LO mode. The shaded rhombohedra show the displacements of the $Q_2$ – type mode. After Ref. 11.

**Acknowledgement**
It is our pleasure to acknowledge many stimulating discussions with K. A. Müller, R. Khasanov, A. Shengelaya, A. R. Bishop, and A. Simon.

**References**

[1] Bednorz J G and Müller K A 1986 *Z. Phys.: Cond. Mat.* **64** 189
[2] Müller K A in *Magnetic Resonance and Relaxation* ed Blinc R 1966, North Holland Publ. Inc. 192
[3] Höck K H, Nickisch H and Thomas H 1983 *Helv. Phys. Acta* **56** 237
[4] Keller H in *Superconductivity in Complex Systems* ed Müller KA and Bussmann-Holder A 2005 *Springer Series Structure and Bonding* **114** 143 and refs. therein
[5] RubioTemprano D, Mesot J, Janssen S, Conder K, Furrer A, Mutka H and Müller K A 2000 *Phys. Rev. Lett.* **84** 1990
[6] Zhao G M and Morris D E 1995 *Phys. Rev. B* **51** 16487
[7] Zhao G M, Hunt M B, Keller H and Müller K A 1997 *Nature (London)* **385** 236
[8] Hofer J, Conder K, Sasagawa T, Zhao G M, Willemin M, Keller H and Kishio K 2000 *Phys. Rev. Lett.* **84** 4192
[9] Khasanov R, Eshchenko D G, Luethens H, Morenzoni E, Prokscha T, Suter A, Garifianov N, Mali M, Roos J, Conder K and Keller H 2004 *Phys. Rev. Lett.* **92** 057602;
[10] Khasanov R, Strässle S, Conder K, Pomjakushina E, Bussmann-Holder A and Keller H (preprint arXiv:0710.5053)

[11] Bussmann-Holder A and Keller H 2005 *Europ. Phys. J* **44** 487
[12] Bussmann-Holder A, Keller H, Bishop A R, Simon A, Micnas R and Müller K A 2005 *Europhys. Lett.* **72**, 423
[13] Bussmann-Holder A and Keller H 2007 *Polarons in Advanced Materials* ed. Alexandrov E S 599
[14] Bishop A R, Bussmann-Holder A, Dolgov O V, Furrer A, Kamimura H, Keller H, Khasanov R, Kremer R K, Manske D, Müller K A and Simon A 2007 *J. Supercond. and Novel Magnetism* **20** 393
[15] Schneider T and Keller H 1992 *Phys. Rev. Lett.* **69** 3374
[16] Alexandrov A S 1992 *Phys. Rev. B* **46** 149332
[17] Bill A, Kresin V Z and Wolf S A 1998 *Phys. Rev. B* **57** 10814
[18] Kamimura H, Hamada T, Matsuno S and Ushio H 2002 *J. Supercond. and Novel Magnetism* **15** 379
[19] Cardona M, Liu R, Thomsen C, Kress W, Schönherr E, Bauer M, Genzel L and König W 1988 *Solid State Comm.* **67** 789
[20] Zech D, Keller H, Conder K, Kaldis E, Liarokapis E, Poulakis N and Müller K A 1994 *Nature (London)* **371** 681
[21] Khasanov R, Shengelaya A, Morenzoni E, Angst M, Conder K, Savić I M, Lampakis D, Liarokapis E, Tatsi A and Keller H 2003 *Phys. Rev. B* **68** 220506 (R)
[22] Khasanov R, Shengelaya A, Morenzoni E, Conder K, Savić I M and Keller H 2004 *J. Phys. Cond. Mat.* **16** S4439
[23] Shengelaya A, Zhao G M, Aegerter C M, Conder K, Savić I M and Keller H 1999 *Phys. Rev. Lett.* **83**, 5142
[24] Khasanov R, Shengelaya A, Di Castro D, Morenzoni E, Maisuradze A, Savić I M, Conder K, Pomjakushina E and Keller H (*preprint arXiv:0711.2257*)
[25] Müller K A 1995 *Nature (London)* **377** 133
[26] Müller K A and Keller H in *High $T_c$ Superconductivity 1996: Ten Years after the Discovery* 1997 Kluwer Academic Publ. 7
[27] Khasanov R, Shengelaya A, Maisuradze E, La Mattina F, Bussmann-Holder A, Keller H and Müller K A 2007 *Phys. Rev. Lett.* **98**, 057007
[28] Khasanov R, Strässle S, Di Castro D, Masui T, Miyasaka S, Tajima S, Bussmann-Holder A and Keller H 2007 *Phys. Rev. Lett.* **99**, 237601
[29] Khasanov R, Shengelaya A, Karpinski J, Bussmann-Holder A, Keller H und Müller K A 2007 *J. Supercond. Novel Magnetism* online 21.12.2007
[30] Carrington A and Manzano F 2003 *Physica (Amsterdam)* **385C**, 205
[31] Oyanagi H, Siani N L, Tsukuda A and Naito M 2006 *J. Phys. Chem. Solids* **67** 2154
[32] McQueeney R J, Petrov Y, Egami T, Yethiraj M, Shirane G and Endoh Y 1999 *Phys. Rev. Lett.* **82** 628
[33] Bianconi A, Saini N L, Lanzara A, Missori M, Rossetti T, Oyanagi H, Yamaguchi H, Oka K and Ito T 1996 *Phys. Rev. Lett.* **76** 3412
[34] Goodenough J B, Zhou J S and Chan J 1993 *Phys. Rev. B* **47** 6275
[35] Bussmann-Holder A, Müller K A, Micnas R, Büttner H, Simon A, Bishop A R and Egami T 2001 *J. Phys. Cond. Mat.* **13** L 168
[36] Lang S G and Firsov Yu A 1963 *Sov. Phys. JETP* **16** 1302
[37] Bussmann-Holder A, Micnas R and Bishop A R 2003 *Europ. Phys. J.* **37** 345
[38] Kohen A, Leibowitch G and Deutscher G 2003 *Phys. Rev. Lett.* **90** 207005
[39] Bussmann-Holder A, Khasanov R, Shengelaya A, Maisuradze A, La Mattina F, Keller H and Müller K A 2007 *Europhys. Lett.* **77** 27002
[40] Kochelaev B I, Sichelschnmidt J, Elschner B, Lemor W and Loidl A 1997 *Phys. Rev. Lett.* **79**, 4274